ISBN: 978-3-95450-247-9 ISSN: 2673-5490 doi: 10.18429/JACoW-IPAC2024-MOPC18

SIMULATED IMPACT OF THE HL-LHC BEAM ON A GRAPHITE TARGET

I. M. Hjelle*, F. Carra, J. Heron, A. Lechner, M. Pasquali[1], A. Piccini, C. Wiesner, D. Wollmann
CERN, Geneva, Switzerland
[1] also at University La Sapienza, Rome, Italy

Abstract

In the High Luminosity Large Hadron Collider (HL-LHC) era, the intensity of the circulating bunches will increase to 2.2×10^{11} protons per bunch, almost twice the nominal LHC value. Besides detailed studies of known and new failure cases for HL-LHC, it is also required to investigate failures beyond nominal design. A consequence of such failures can be the impact of a large number of high-energy particles in one location, resulting in a significantly increased damage range due to an effect called hydrodynamic tunnelling. This phenomenon is studied by coupling FLUKA, an energy deposition code, and Autodyn, a hydrodynamic code.

This paper presents the simulated evolution of the deposited energy, density, temperature and pressure for the impact of the HL-LHC beam on a graphite target. It then computes the resulting tunnelling range and finally compares the outcome with previous studies using LHC intensities.

INTRODUCTION

Complementary to the study of known and new failure cases [1] for the High Luminosity Large Hadron Collider (HL-LHC) [2], the consequences of failures beyond design have to be assessed. A worst-case, beyond-design failure is the impact of the entire beam at a single point. Successive proton bunches impacting at one point on a target create high pressure and temperature. This depletes the material density along the beam path, allowing the particle showers created by subsequent proton bunches to penetrate deeper into the target. This results in an increased longitudinal damage range for a beam of proton bunches when compared to a single bunch of the same energy. The phenomenon is known as hydrodynamic tunnelling [3–5] and has been studied extensively for the LHC [6–10].

In the HL-LHC era, the bunch intensity at the start of collision will increase to 2.2×10^{11} protons per bunch [2], almost twice the nominal LHC intensity of 1.15×10^{11} protons per bunch [11]. Two studies using HL-LHC beam parameters and two different rms beam sizes of 0.5 mm and 1.0 mm are conducted. The beam impact is simulated by coupling the energy-deposition code FLUKA [12–14] and the hydrodynamic code ANSYS Autodyn [15] sequentially [16,17]. This paper presents the results of the two studies and compares them to the previous LHC study [6].

SIMULATION SETUP AND PARAMETERS

The beam parameters used for the simulation are presented in Table 1 [2]. Filling scheme details are neglected and a constant bunch spacing of 25 ns is assumed. With 2760 bunches, this results in a total beam impact time of 69 μs. The beam size $\sigma = 0.5$ mm is chosen as it is identical to previous LHC studies [6, 8], while $\sigma = 1.0$ mm is simulated to study the effect of doubling the beam size in both planes.

Table 1: Beam Parameters Used in the HL-LHC Simulations

Beam Energy	7 TeV
Total number of bunches	2760
Protons per bunch	2.2×10^{11}
Bunch spacing	25 ns
rms beam size (σ)	0.5 mm, 1.0 mm

To facilitate comparison with the previous LHC study [6], the same material and target parameters are used for the FLUKA simulation, as summarised in Table 2. Furthermore, the radial and longitudinal segmentation of the target are kept identical to [6, 7].

Table 2: Target Parameters

Target length	10 m
Target radius	5 cm
Material	Graphite
Initial target density	2.28 g cm^{-3}

SIMULATION WORKFLOW

The FLUKA simulation yields an energy deposition map. This map is then used as input for the subsequent Autodyn simulation. The Autodyn simulation uses a tabular equation of state from the SESAME library, and an Eulerian mesh, the same as used for the LHC study [6]. More details can be found in [6, 7].

The Autodyn simulation is run until there is a 20% decrease in the minimum value of the target density. When this occurs, the density distribution of the material is updated in FLUKA using a coupling script [16, 17]. The FLUKA simulation is then rerun, and the generated map of the energy deposition per proton is scaled to the total number of protons per bunch before being used as input for the subsequent Autodyn simulation.

This loop continues until the minimum density drops below a predefined threshold of 0.5 g cm^{-3} and the speed of the density depletion front becomes constant. From this point on, the Autodyn simulation is run for a predefined constant time of 1.25 μs per coupling step. This timestep is chosen as it is equivalent to half the timestep used in the LHC study. As the intensity is almost doubled, this leads to a similar energy deposition per time step.

* ingrid.midtbust.hjelle@cern.ch

ISBN: 978-3-95450-247-9 ISSN: 2673-5490 doi: 10.18429/JACoW-IPAC2024-MOPC18

RESULTS

The longitudinal energy-deposition profile at the target axis is depicted in Fig. 1 for different time steps. The simulation is performed with HL-LHC beam intensities for the rms beam sizes 0.5 mm (Fig. 1a) and 1.0 mm (Fig. 1b). Each line represents a timestep at which the FLUKA density map is updated.

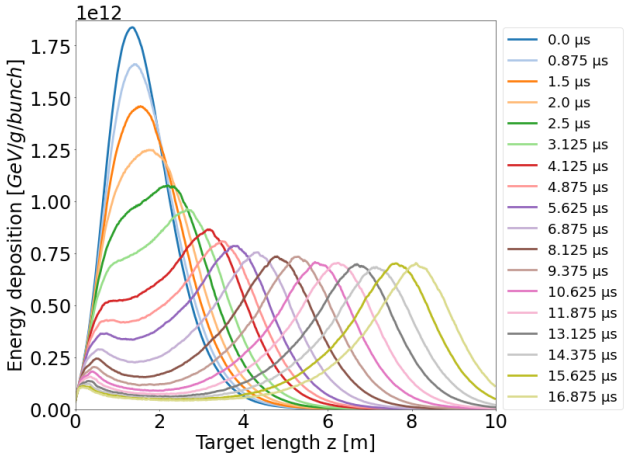

(a) σ = 0.5 mm.

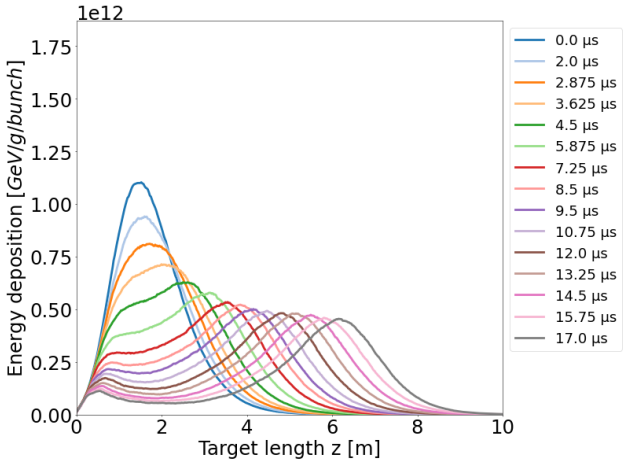

(b) σ = 1.0 mm.

Figure 1: Time evolution of the energy deposition at the target axis (r <125 μm) for σ = 0.5 mm (top) and σ = 1.0 mm (bottom).

For the HL-LHC 0.5 mm study, the maximum value of the initial energy deposition peak is 1.8×10^{12} GeV/g/bunch, located longitudinally 1.35 m from the beginning of the target. The corresponding values for the HL-LHC 1.0 mm study are 1.1×10^{12} GeV/g/bunch for the initial peak located at 1.53 m. After the impact of subsequent bunches, the peak energy deposition decreases. This is due to the density depletion along the axis which allows the energy to be deposited further into the material. Two peaks develop, one at the beginning of the material, and one propagating longitudinally into the material. The second peak converges to an equilibrium value, as seen in Fig. 1. This value is reached after 4.125 μs for the HL-LHC 0.5 mm beam, and after 5.875 μs for the HL-LHC 1.0 mm beam.

Density Depletion Speed and Tunnelling Range

Once the energy deposition peak has reached its equilibrium value, it will continue to propagate deeper into the target at a constant speed. In the same manner, the density depletion front will also reach a constant propagation speed. As a change in density can be associated with material damage, this propagation speed has been utilized in prior research [3, 6] to estimate the total tunnelling range by considering the propagation speed at one density level. A similar approach is applied in this study, however, an average over 20 density levels between 1.5 g cm^{-3} and 2.0 g cm^{-3} is taken. Only timesteps after the energy deposition reaches its equilibrium value are used. This is illustrated in Fig. 2 with the transition from dashed to solid lines after 4.125 μs.

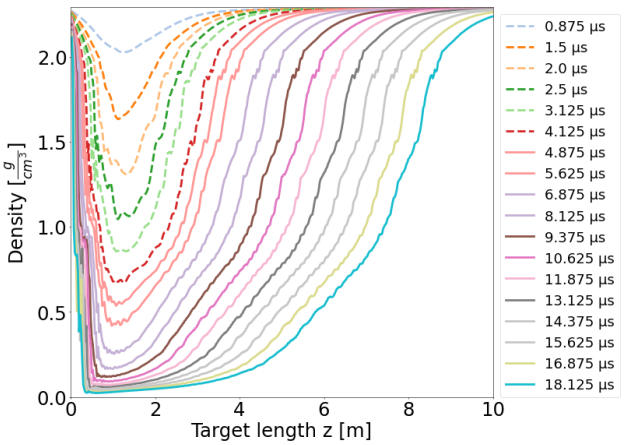

Figure 2: Time evolution of the density at the target axis (r <125 μm) after the impact of the HL-LHC 0.5 mm beam.

The total tunnelling range is found by adding the range reached after 4.125 μs to the range obtained by multiplying the calculated propagation speed with the remaining beam impact time (69 μs - 4.125 μs). The results are presented in Table 3. The values for the LHC study have been recalculated by applying the same method to the data of the last study. For better comparison, it is chosen to also extrapolate the LHC beam to 2760 bunches as opposed to the previously used 2808 bunches [6]. The uncertainties in Table 3 correspond to the standard deviation due to averaging over the different density levels, and do not include systematic errors, which will be assessed in more detail in the future.

When comparing LHC and HL-LHC intensities for the same beam size of 0.5 mm, the tunnelling range increases by ~45%. For HL-LHC intensities, increasing the beam size from 0.5 mm to 1.0 mm in both planes results in a decrease of ~37% in the tunnelling range.

Interestingly, the impact of the LHC 0.5 mm beam and the HL-LHC 1.0 mm beam leads to similar calculated tunnelling ranges. This is hypothesised to result from a similar maximum initial energy deposition per bunch, reached at the target axis.

ISBN: 978-3-95450-247-9 ISSN: 2673-5490 doi: 10.18429/JACoW-IPAC2024-MOPC18

Table 3: Resulting Tunnelling Speed, Tunnelling Range, and Maximum Initial Energy Deposition, for LHC and HL-LHC Parameters

Protons per bunch [10^{11}]	**1.15**	**2.2**	**2.2**
Beam sigma [mm]	0.5	0.5	1.0
Tunnelling speed [$\frac{\text{cm}}{\mu\text{s}}$]	25.1 $\pm$ 0.7	38.0 $\pm$ 1.6	26.3 $\pm$ 1.1
Tunnelling range [m]	20.5 $\pm$ 0.5	29.6 $\pm$ 0.6	21.6 $\pm$ 0.4
Maximum initial energy deposition [$10^{12} \cdot \frac{\text{GeV}}{\text{g·bunch}}$]	1.0	1.8	1.1

Comparison with LHC

Figure 3 compares the density (Fig. 3a), temperature (Fig. 3b) and pressure (Fig. 3c) 14.2 μs after the start of the beam impact for the previous LHC study [6] and the two HL-LHC studies. The timestep is the final one for the LHC study, and for better comparison, it is chosen to depict the same timestep for the two HL-LHC studies.

In Fig. 3a, the HL-LHC 0.5 mm beam reaches significantly deeper into the material, which is due to the higher tunnelling speed. The HL-LHC 1.0 mm beam and the LHC 0.5 mm beam cause a similar density depletion, however, for the HL-LHC 1.0 mm beam the density depletion reaches slightly further into the material, consistent with the slightly higher tunnelling speed and slightly higher maximum initial energy deposition.

A main aspect to note from Fig. 3 is the correlation between all hydrodynamic parameters in the longitudinal direction. Looking at the temperature (Fig. 3b), the flat plateau represents the phase transition into the two-phase gas-liquid state [3]. The part above the plateau, which is the gas state, corresponds well to the part of the material where the density approaches zero. At the plateau, a higher gradient is observed in the density, and at the end of the plateau, the density quickly approaches its initial value. Similar observations can be made for the pressure (Fig. 3c). The longitudinal range with maximum pressure corresponds to the plateau. In this range, pressure oscillations are observed. These are believed to be correlated to the phase transition in the material.

In Fig. 3c, the amplitude of the pressure is significantly lower for the LHC study than for both HL-LHC studies, suggesting that at least for these specific simulation parameters, the peak pressure is not related to the beam size but to bunch intensity. This implies that the pressure is not a localized phenomenon on the target axis but driven by the total deposited energy.

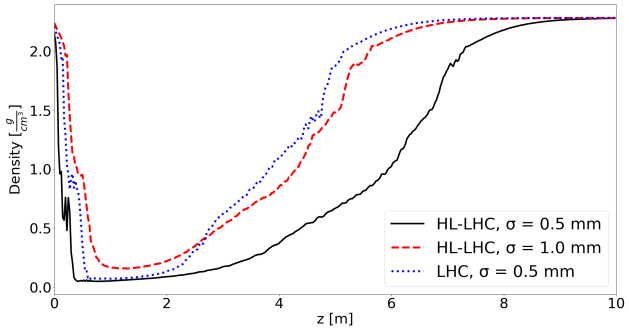

(a) Density.

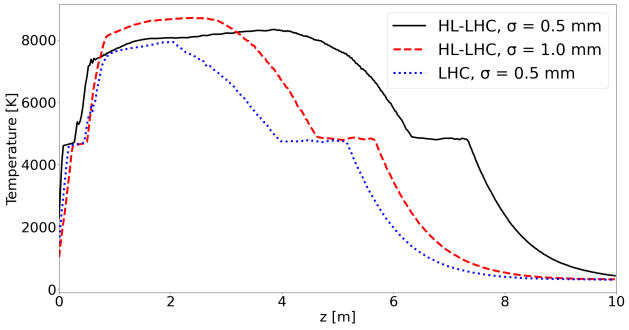

(b) Temperature.

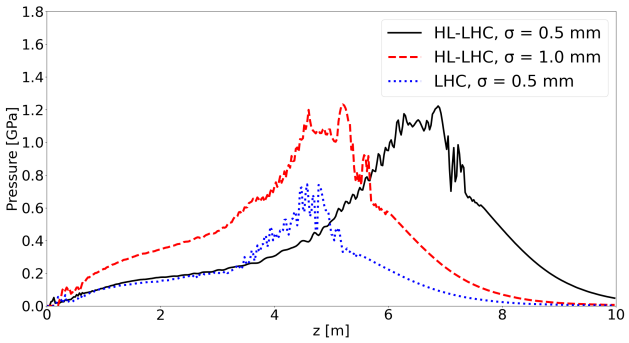

(c) Pressure.

Figure 3: Comparison of density, temperature and pressure for all studies after 14.2 μs at $r < 125$ μm.

CONCLUSIONS

Using HL-LHC intensities, the worst-case scenario of a direct beam impact on a graphite target is simulated for two different rms beam sizes by coupling the numerical codes FLUKA and ANSYS Autodyn. The total tunnelling range for the impact of the full HL-LHC beam was estimated to be 29.6 m $\pm$ 0.6 m for a beam size of 0.5 mm and 21.6 m $\pm$ 0.4 m for a beam size of 1.0 mm. Compared to previous results with LHC parameters [6], the tunnelling range increases by ~45% when almost doubling the bunch intensity from LHC nominal to HL-LHC values, considering the same beam size of 0.5 mm.

ACKNOWLEDGEMENTS

This research was supported by the HL-LHC project. The authors would like to thank R. Schmidt, N. Tahir, and Y. Nie for valuable discussions about hydrodynamic tunnelling, J. Kruse-Hansen, I. Kolthoff, R. Rasile, and J. Don for their contributions to the coupling scripts and establishing the simulation workflow, as well as D. Gancarcik and C. Hernalsteens for support in the efficient use of computational resources.

ISBN: 978-3-95450-247-9 ISSN: 2673-5490 doi: 10.18429/JACoW-IPAC2024-MOPC18

REFERENCES

[1] B. Lindstrom *et al.*, "Fast failures in the LHC and the future high luminosity LHC", *Phys. Rev. Accel. Beams*, vol. 23, no. 8, p. 81001, Aug. 2020. doi:10.1103/PhysRevAccelBeams.23.081001

[2] I. Béjar Alonso *et al.*, "High-Luminosity Large Hadron Collider (HL-LHC): Technical design report", CERN, Geneva, Switzerland, 2020, Rep. CERN-2020-010. doi:10.23731/CYRM-2020-0010

[3] N. A. Tahir *et al.*, "Review of hydrodynamic tunneling issues in high power particle accelerators", *Nucl. Instrum. Methods B*, vol. 427, Jul. 2018, pp. 70–86. doi:10.1016/j.nimb.2018.04.009

[4] Y. Nie *et al.*, "Simulation of hydrodynamic tunneling induced by high-energy proton beam in copper by coupling computer codes", *Phys. Rev. Accel. Beams*, vol. 22, p. 014501, Jan. 2019. doi:10.1103/PhysRevAccelBeams.22.014501

[5] A. Bertarelli, "Beam-Induced Damage Mechanisms and their Calculation", *CERN Yellow Reports: Monographs*, CERN, Geneva, Switzerland, Rep. CERN-2016-002, pp.159-227, 2016. doi:10.5170/CERN-2016-002.159

[6] C. Wiesner *et al.*, "Study of hydrodynamic-tunnelling effects induced by high-energy proton beams in graphite", *J. Phys.: Conf. Ser.*, vol. 2420, p. 012004, 2023. doi:10.18429/JACoW-IPAC2022-WEPOPT015

[7] J. Don and C. Wiesner, "Simulation of hydrodynamic tunnelling effects induced by 7 TeV protons in graphite", CERN, Geneva, Switzerland, Tech. Note 2739903, May 2022. https://edms.cern.ch/document/2739903

[8] N. A. Tahir *et al.*, "Impact of high energy high intensity proton beams on targets: Case studies for Super Proton Synchrotron and Large Hadron Collider", *Phys. Rev. Accel. Beams*, vol. 15, p. 051003, May 2012. doi:10.1103/PhysRevSTAB.15.051003

[9] J. Blanco Sancho, "Machine Protection and High Energy Density States in Matter for High Energy Hadron Accelerators", Ph.D. Thesis, École Polytechnique Fédérale de Lausanne, Lausanne, Switzerland, 2014. https://cds.cern.ch/record/1704466

[10] F. Burkart, "Expected damage to accelerator equipment due to the impact of the full LHC beam: beam instrumentation, experiments and simulations", Ph.D. Thesis, Fachbereich Physik der Goethe-Universit, Frankfurt, Germany, 2016. https://cds.cern.ch/record/2229595

[11] O. Bruning, P. Collier, P. Lebrun, S. Myers, R. Ostojic, J. Poole, P. Proudlock, "LHC Design Report", CERN, Geneva, Switzerland, Rep. CERN-2004-003-V-1, 2004. doi:10.5170/CERN-2004-003-V-1

[12] CERN, "FLUKA", https://fluka.cern/

[13] G. Battistoni *et al.*, "Overview of the FLUKA code", *Ann. Nucl. Energy 82*, pp. 10–18, 2015. doi:10.1016/j.anucene.2014.11.007

[14] C. Ahdida *et al.*, "New Capabilities of the FLUKA Multi-Purpose Code", *Front. Phys.*, vol. 9, 2022. doi:10.3389/fphy.2021.788253

[15] ANSYS Autodyn, "ANSYS Inc.". https://www.ansys.com/products/structures/ansys-autodyn

[16] C. Wiesner, F. Carra, J. Kruse-Hansen, M. Masci, Y. Nie, and D. Wollmann, "Efficient Coupling of Hydrodynamic and Energy-Deposition Codes for Hydrodynamic-Tunnelling Studies on High-Energy Particle Accelerators", in *Proc. IPAC'21*, Campinas, Brazil, May 2021, pp. 119–122. doi:10.18429/JACoW-IPAC2021-MOPAB024

[17] I. Kolthoff, "Coupling script for hydrodynamic-tunnelling studies", 2021. https://gitlab.cern.ch/machine-protection/hydrodynamic-tunnelling/coupling-script-lhc-carbon